CrystEngComm

Accepted Manuscript

ROYAL SOCIETY OF CHEMISTRY

www.rsc.org/crystengcomm

Journal Name

COMMUNICATION

Topochemical transformation of low energy crystal facets to high energy facets: A case from $Bi_2O_2CO_3$ {001} facets to β-Bi_2O_3 {001} facets with improved photocatalytic oxidation of NO†

Received 00th January 20xx,
Accepted 00th January 20xx

DOI: 10.1039/x0xx00000x

www.rsc.org/

Fang Wang,[a,b] Ziyan Zhao,[b] Kunhao Zhang,[c] Fan Dong,[d] and Ying Zhou[a,b*]

Abstract. Herein, β-Bi_2O_3 nanosheets exposed with active {001} facets was facilely prepared through annealing $Bi_2O_2CO_3$ with thermal stable {001} facets. The enhanced photocatalytic activity of β-Bi_2O_3 was ascribed to the high energy of {001} facets and the efficient charge separation. This 2D surface transformation strategy shed new light on the fabrication of energetic facets and the development of highly active photocatalyst.

Since the successful synthesis of high energy {001} facets of anatase TiO_2 crystals using HF as a controlling agent,[1] semiconductor crystal-facet engineering is becoming a hot research topic in the pursuit of highly reactive faceted photocatalysts.[2] Generally, Semiconductor crystals exposed with different facets have diverse physicochemical properties and result in very different catalytic activities. For instance, BiOCl nanosheets with exposed {001} facets exhibited enhanced photoactivity compared to the counterpart with {010} facets.[3] The improved photocatalytic activity of Ag_3PO_4 rhombic dodecahedrons has been ascribed to the higher energy of {110} facets (1.31 J/m^2) than of {100} facets (1.12 J/m^2).[4] However, controlling the crystal facets of semiconductors is still a tremendous challenge, which has only been achieved in limited material systems.[1,5] So far, almost all of these semiconductors with controlled surface facets were obtained by hydrothermal methods.[1-5] As the reactive facets diminish rapidly during the crystal growth due to the minimization of surface energy, optimizing the reaction kinetics is crucial which may require considerable "trial and error" work.[6] Therefore, the predictive and rational preparation of a desired crystal facet is rather difficult. This calls for the development of novel preparative strategy.

Sillén-type $Bi_2O_2CO_3$ is composed of alternating $Bi_2O_2^{2+}$ and CO_3^{2-} layers along *c* axis. Consequently, $Bi_2O_2CO_3$ nanosheets dominated with {001} facets have been easily prepared by various groups.[7] Meanwhile, metastable β-Bi_2O_3 has closely related crystal structure with $Bi_2O_2CO_3$ because both of them contain the same atomic arrangement of the $Bi_2O_2^{2+}$ layers.[8] Especially, the lattice misfit between {110} facets of $Bi_2O_2CO_3$ and {220} facets of β-Bi_2O_3 is only 0.1%,[9] indicating that these two phases could be transformed with each other easily. It was found that even under room temperature β-Bi_2O_3 can capture atmospheric CO_2 to form $Bi_2O_2CO_3$ nanosheets in our previous work.[10] Meanwhile, $Bi_2O_2CO_3$ can convert back to metastable β-Bi_2O_3 through releasing CO_2 by annealing.[11] Nevertheless, compared to $Bi_2O_2CO_3$, β-Bi_2O_3 nanosheets with exposed {001} facets have been seldom reported due to the high surface energy of {001} facets (1.83 J/m^2), which is higher than both of {100} (0.98 J/m^2) and {110} (1.42 J/m^2) facets.[12]

In this work, we report a facile route to fabricate the energetic facet via lattice matching, i.e., the reactive facet of one crystal can be prepared by another material with thermodynamically stable facet through annealing. β-Bi_2O_3 and $Bi_2O_2CO_3$ were selected as model materials as they have close crystal structure and well lattice match. This concept could have a good universality in the synthesis of other high reactive faceted materials and shed light on the development of high active photocatalyst.

The detailed procedure for the theoretical calculations and experiments was described in ESI. Fig. S1 shows the structures of $Bi_2O_2CO_3$ and β-Bi_2O_3 with side view of (001), (110) and (010) facets. The surface free energies of these stoichiometric low miller index surfaces for both $Bi_2O_2CO_3$ and β-Bi_2O_3 were computed through density functional theory (DFT) calculations. It was observed that the variation trend is the same for the surface free energies with and without surface relaxation (Table 1) in accordance with the previous theoretical surface study on bismuth oxides.[13] The (001) facet of $Bi_2O_2CO_3$ has the lowest surface free energy compared to other planes, while for β-Bi_2O_3 the (001) facet exhibits the highest surface free energy. Therefore, it is proved that the experimental preparation of β-Bi_2O_3 with energetic {001} facets is much more difficult than that of $Bi_2O_2CO_3$ with thermodynamically stable {001} facets. Fig. 1 highlights the structure details related to atomic arrangements. It is interesting to note that they have a common

[a] State Key Laboratory of Oil and Gas Reservoir Geology and Exploitation, Southwest Petroleum University, Chengdu 610500, China. E-mail: yzhou@swpu.edu.cn
[b] The Center of New Energy Materials and Technology, School of Materials Science and Engineering, Southwest Petroleum University, Chengdu 610500, China
[c] Shanghai Synchrotron Radiation Facility, Shanghai Institute of Applied Physics, Chinese Academy of Science, Shanghai 201204, China
[d] College of Environmental and Biological Engineering, Chongqing Technology and Business University, Chongqing 400067, China
† Electronic Supplementary Information (ESI) available: [Experimental details, and Fig. S1 to S5]. See DOI: 10.1039/x0xx00000x

structural feature along the (001) plane. The atomic array of $Bi_2O_2^{2+}$ layer in $Bi_2O_2CO_3$ is also the same fragment existing in β-Bi_2O_3, which means the Bi and O atom fragment in $Bi_2O_2^{2+}$ of $Bi_2O_2CO_3$ is prone to rearrange to form β-Bi_2O_3 along the (001) facet after releasing CO_2. The two-dimensional (2D) surface transformation along the (001) plane could result in the same lattice arrays for $Bi_2O_2CO_3$ and β-Bi_2O_3. Therefore, β-Bi_2O_3 nanosheets with active {001} facets could be prepared from the easily accessed $Bi_2O_2CO_3$ with exposed {001} facets.

Table 1 Calculated surface energies (in J/m^2) with and without surface relaxation of various facets for $Bi_2O_2CO_3$ and β-Bi_2O_3.

crystal	(001)	(110)	(010)
$Bi_2O_2CO_3$	1.23 (1.01)*	1.37 (1.00)	1.79 (1.15)
β-Bi_2O_3	1.96 (0.57)	1.43 (0.21)	1.44 (0.22)

* Data in parentheses refer to the surface energy with surface relaxation.

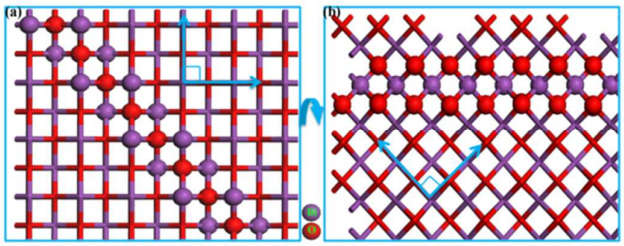

Fig. 1 Atomic arrays of $Bi_2O_2^{2+}$ layers of (a) $Bi_2O_2CO_3$ and (b) β-Bi_2O_3 top-viewed along (001) facet.

Inspired by the theoretical calculations, $Bi_2O_2CO_3$ (BOC) particles were prepared through modifying a reported method.[14] The TG curve (Fig. S2) reveals that the obtained BOC samples start to decompose at 340 °C and ca. 8% weight loss is observed, matching well with the theoretical weight loss (8.6%) due to the releasing of CO_2. Consequently, the obtained samples were annealed under atmosphere at 350, 380, 400 and 420 °C, respectively, which are denoted as BOC-350, BOC-380, BOC-400 and BOC-420. Fig. S3 shows the PXRD patterns of these samples. All diffraction peaks of the prepared BOC can be indexed into the tetragonal $Bi_2O_2CO_3$ (JCPDS No. 41-1488). Although tetragonal β-Bi_2O_3 was already formed at 350 °C, BOC-350 is still dominated by $Bi_2O_2CO_3$ phase. With further increasing the temperature, the ratio of β-Bi_2O_3 in the products (BOC-380 and BOC-400) increased. Finally, $Bi_2O_2CO_3$ was completely converted to β-Bi_2O_3 phase (BOC-420) at 420 °C. In addition, tiny amount of $Bi_2O_{2.33}$ was observed as well. As β-Bi_2O_3 is a metastable phase, it could convert to thermodynamic stable α-Bi_2O_3 phase under higher annealing temperature.[15] In line with the PXRD patterns, the UV-vis absorption spectra of these samples also varied with the temperatures (Fig. S4). The band gap (E_g) of BOC, BOC-350, BOC-380, BOC-400 and BOC-420 was determined as 3.55, 3.29, 2.58, 2.52 and 2.52, respectively, according to the onset of the absorption edge. The E_g of BOC matched well the previous reported value of $Bi_2O_2CO_3$,[16] whereas the E_g of these samples decreased with the annealing temperatures as the E_g of β-Bi_2O_3 is much smaller than that of $Bi_2O_2CO_3$.[17]

To get insight into the chemical states of the elements on the surface of BOC and BOC-420, XPS spectra were performed. Both samples contained Bi, O and C in the survey spectra (Fig. 2a). Fig. 2b shows two strong symmetrical peaks at ca. 164.4 and 159.1 eV, corresponding to Bi $4f_{5/2}$ and Bi $4f_{7/2}$ signals from Bi^{3+} ions for both samples.[18] Fig. 2c displays the O1S spectra of BOC and BOC-420. A broad peak range from 529 to 534 was observed, which can be fitted by three peaks at binding energies of 530.6, 531.6 and 532.6 eV for BOC or 530.1, 531.1 and 531.8 eV for BOC-420. The peak at 530.6 (530.1) eV can be ascribed to the oxygen of Bi-O bond, while the other two peaks are from the lattice oxygen and carbonate species and adsorbed H_2O on the surface.[19] The peaks for C 1s located at 284.8, 285.6 and 286.7 eV are ascribed to adventitious carbon species from the XPS instrument, whereas the peak at 289.0 eV can be assigned to the carbon in the CO_3^{2-} group (Fig. 2d).[20] These results revealed that even after annealing at 420 °C, the surface of BOC-420 still contained CO_3^{2-}, which could play an important role in the stabilization of metastable β-Bi_2O_3. Previously, Jang et al found that β-Bi_2O_3 converted to thermally stable α-Bi_2O_3 phase once the remaining surface-coordinated CO_3^{2-} was not enough to stabilize the crystal structure of β-Bi_2O_3.[15]

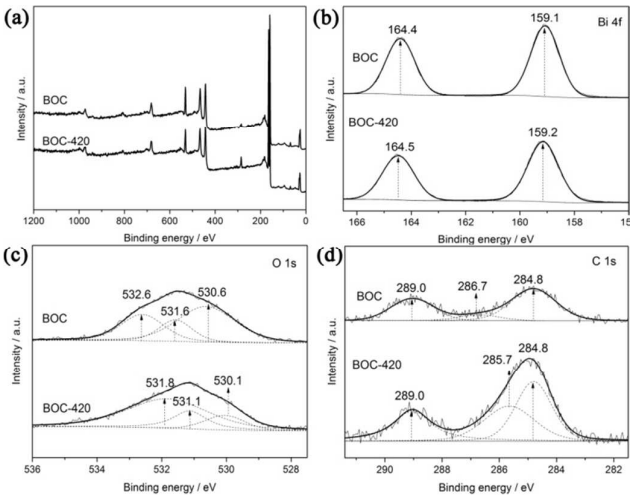

Fig. 2 XPS spectra of (a) survey; (b) Bi4f; (c) O1S; (d) C1s for BOC and BOC-420.

The morphology and microstructure of these samples were further investigated by SEM and TEM observations. The prepared BOC is constituted by large amounts of nanosheets with thickness ca. 30 nm (Fig. 3a and 3b). Annealing at 420 °C did not significantly change the morphology and size of the products. Hence, BOC-420 could maintain the 2D morphology of BOC (Fig. 3c and 3d). TEM images (Fig. 4a and 4c) further confirmed the similar 2D morphology for both BOC and BOC-420. The BET surface areas of BOC and BOC-420 were determined as 14.3 and 5.9 m^2/g, respectively. The HRTEM image of BOC (Fig. 4b) shows clear lattice fringes with an interplanar lattice spacing of 0.274 nm and an angle of 90°, which is consistent with the (110) planes of the tetragonal $Bi_2O_2CO_3$. The corresponding SAED pattern (inset of Fig. 4b) indicates the single-crystal nature of BOC, which can be indexed as the [001] zone axis. Both HRTEM and SAED results confirmed that

the top and bottom exposing surface of BOC are {001} facets. According to Fig. 1, β-Bi_2O_3 and $Bi_2O_2CO_3$ have similar atomic arrays of $Bi_2O_2^{2+}$ layers along (001) facets. Hence, β-Bi_2O_3 with active {001} facets could be transformed from $Bi_2O_2CO_3$ with exposed {001} facets through annealing. Fig. 4d shows the HRTEM image of BOC-420. A lattice fringe of 0.274 nm was observed, corresponding to the interplanar spacing of the (220) of tetragonal β-Bi_2O_3. The angle of adjacent spots marked in the SAED pattern is 45°, matching well with the theoretical value of the angle between the (220) and (200) planes of β-Bi_2O_3. Therefore, the set of diffraction spots can be assigned to the [001] zone-axis diffraction spots of β-Bi_2O_3, revealing that β-Bi_2O_3 nanosheets with exposed {001} facets have been successfully obtained through annealing $Bi_2O_2CO_3$ nanosheets with {001} facets at 420 °C. We believe the lattice match between {110} facets of $Bi_2O_2CO_3$ and {220} facets of β-Bi_2O_3 is the main reason for the formation of β-Bi_2O_3 with active {001} facets. On the other hand, the CO_3^{2-} content on the surface of β-Bi_2O_3 (Fig. 2d) may also play an important role, which can lower the surface energy of β-Bi_2O_3.[15] Similar phenomenon has been reported in other material systems. For example, anatase TiO_2 with active {001} facets can be prepared in the presence of F^- because the surface adsorbed F^- is effective to lower the surface energy of {001} surface of anatase TiO_2.[1,2,21]

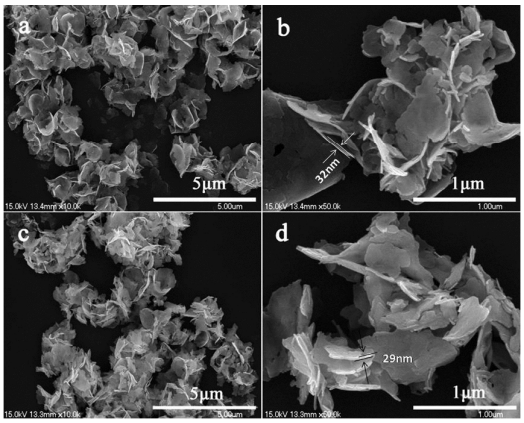

Fig. 3 Representative SEM images of (a) BOC (low magnification); (b) BOC (high magnification); (c) BOC-420 (low magnification); (d) BOC-420 (high magnification).

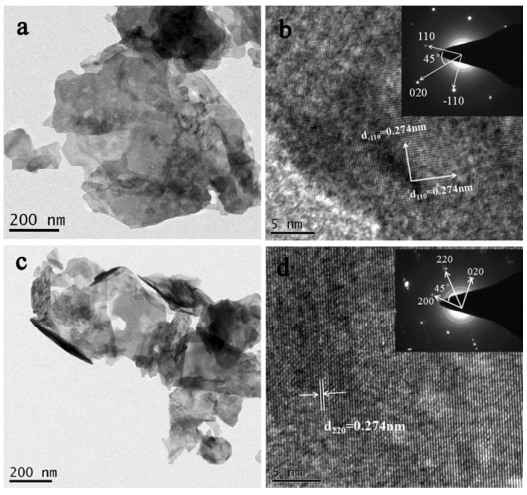

Fig. 4 TEM images of (a) BOC and (c) BOC-420; HRTEM images of (b) BOC and (d) BOC-420 (Insets are the corresponding SAED patterns).

Photocatalytic activity of these samples was evaluated by photocatalytic oxidation of ppb-level NO in air under UV-visible and visible light (λ > 420 nm) irradiation. As shown in Fig. 5, after 30 min irradiation, the NO removal ratio of BOC under UV-visible light is 41%, while it is only 19% under visible light irradiation due to the large band gap (Fig. S4). The photocatalytic behaviour of BOC-400 is similar to that of BOC. Importantly, BOC-420 exhibits significantly enhanced NO removal efficiency especially under visible light irradiation. The NO removal ratio over BOC-420 can reach as high as 54% or 40% after 30 min UV-visible light or visible light irradiation, respectively. Generally, conventional TiO_2 (P25) photocatalyst exhibited almost no photocatlytic NO oxidation activity under visible light irradiation due to its wide band gap. Using the same reactor, the photodegradation ratio of NO over P25 under UV light after 30 min irradiation is 38 %.[19] Moreover, the commercial β-Bi_2O_3 particles (sigma-Aldrich) with a particle size range of 90-210 nm and a BET surface area of 3.2-3.5 m^2/g were taken as a reference to compare the activity with the prepared β-Bi_2O_3 with active {001} facets. Fig. S5 shows the XRD and SEM of the commercial particles. The commercial β-Bi_2O_3 particles exhibited a much lower photocatalytic activity compared to BOC-420 both under UV-visible light and visible light irradiation (Fig. 5). All in all, these results confirmed the prepared β-Bi_2O_3 exhibited enhanced photocatlytic activity towards to NO oxidation, which could be attributed to the high energy of {001} facets (1.96 J/m^2) (Table 1), given that both BOC and BOC-420 have similar morphology and particle size (Fig. 3).

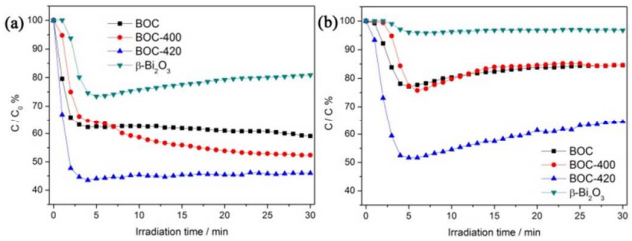

Fig. 5 Photocatalytic activities of the prepared samples and commercial β-Bi_2O_3 nanoparticles as reference under (a) UV-visible light and (b) visible light (λ > 420 nm) irradiation.

Photocurrent measurements were further performed to investigate the interfacial charge transfer behaviours.[22] All of these experiments were measured in a standard three-electrodes photoelectrochemical cell (ESI). BOC exhibited anodic photocurrent generation under both UV-visible light and visible light irradiation, indicating their n-type semiconductor behaviours (Fig. 6). In line with its wide band gap (Fig. S4), the photocurrent of BOC under visible light is very low. However, BOC-380 and BOC-400 exhibited different behaviours. Under visible light irradiation, both of them displayed cathodic photocurrent, revealing their p-type semiconductor property (Fig. 6). β-Bi_2O_3 is a p-type semiconductor.[23] Hence, under visible light irradiation, only the formed β-Bi_2O_3 was activated. Under UV-visible light, an anodic photocurrent was observed for both samples. Consequently, although both $Bi_2O_2CO_3$ and β-Bi_2O_3 can be activated under UV-visible light, the photocurrent was dominated by that from $Bi_2O_2CO_3$. As $Bi_2O_2CO_3$ is a n-type semiconductor, the formation of β-Bi_2O_3 and $Bi_2O_2CO_3$ p-n heterojunctions could reduce the

recombination rate of photogenerated electrons and holes, thus resulting in enhanced anodic photocurrent compared to the pristine $Bi_2O_2CO_3$.[24] After annealing at 420 °C, $Bi_2O_2CO_3$ decomposed completely (Fig. S3). Therefore, only cathodic photocurrent was observed for BOC-420 regardless of UV-visible light or visible light irradiation. Besides, BOC-420 exhibited the highest photocurrent among the studied samples, confirming that β-Bi_2O_3 with active {001} facets also revealed more efficient charge separation compared to $Bi_2O_2CO_3$.

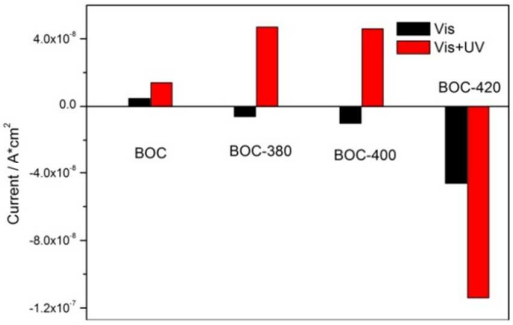

Fig. 6 Photocurrent of the obtained samples under UV-visible light and visible light (λ > 420 nm) irradiation.

Conclusions

In summary, we report a facile route to prepare β-Bi_2O_3 nanosheets with active {001} facets through annealing $Bi_2O_2CO_3$ nanosheet precursor. The lattice match between {110} facets of $Bi_2O_2CO_3$ and {220} facets of β-Bi_2O_3 as well as the CO_3^{2-} content on the surface could be the reason for the formation of β-Bi_2O_3 with active {001} facets. The prepared β-Bi_2O_3 nanosheets exhibited enhanced photocatalytic activity toward to NO oxidation both under UV-visible light and visible light irradiation due to the high energy of {001} facets (1.96 J/m^2) and the more efficient charge separation. This strategy is expected to be applicable to prepare other materials with active facets for photocatalytic applications.

Acknowledgements

This research was funded by the National Natural Science Foundation of China (U1232119), Sichuan Youth Science and Technology Foundation (2013JQ0034, 2014JQ0017), Scientific Research Starting project of SWPU (2014QHZ020, 2014QHZ021, 2014PYZ012), and the Innovative Research Team of Sichuan Provincial Education Department and SWPU (2012XJZT002).

Notes and references

1 H. G. Yang, C. H. Sun, S. Z. Qiao, J. Zoum G. Liu, S. C. Smith, H. M. Cheng and G. Q. Lu, *Nature*, 2008, **453**, 638.
2 (a) G. Liu, J. C. Yu, G. Q. Lu and H. M. Cheng, *Chem. Commun.*, 2011, **47**, 6763; (b) G. Liu, H. G. Yang, J. Pan, Y. Q. Yang, G. Q. Lu and H. M. Cheng, *Chem. Rev.*, 2014, **114**, 9559.
3 J. Jiang, K. Zhao, X. Y. Xiao and L. Z. Zhang, *J. Am. Chem. Soc.*, 2012, **134**, 4473.
4 Y. P. Bi, S. X. Ouyang, N. Umezawa, J. Y. Cao and J. H. Ye, *J. Am. Chem. Soc.*, 2011, **133**, 6490.
5 (a) Y. P. Xie, G. Liu, L. C. Yin and H. M. Cheng, *J. Mater. Chem.*, 2012, **22**, 6746; (b) R. G. Li, F. X. Zhang, D. Wang, J. X. Yang, M. R. Li, J. Zhu, X. Zhou, H. X. Han and C. Li, *Nature Commun.*, 2013, **4**, 1432; (c) J. L. Long, S. C. Wang, H. J. Chang, B. Z. Zhao, B. T. Liu, Y. G. Zhou, W. Wei, X. X. Wang, L. Huang and W. Huang, *Small*, 2014, **10**, 2791; (d) J. M. Peng, Y. Zhou, H. Wang, H. R. Zhou and S. Y. Cai, *CrystEngComm*, 2015, **17**, 1805.
6 (a) K. Byrappa and T. Adschin, *Prog. Cryst. Growth Characterization Mater.*, 2007, **53**, 117; (b) G. R. Patzke, Y. Zhou, R. Kontic, F. Conrad, *Angew. Chem. Int. Ed.,* 2011, **50**, 826; (c) Y. Zhou, N. Pienack, W. Bensch and G. R. Patzke, Small, 2009, 5, 1978; (d) Y. Zhou, E. Antonova, W. Bensch and G. R. Patzke, *Nanoscale*, 2010, **2**, 2412.
7 (a) Y. Zheng, F. Duan, M. Q. Chen and Y. Xie, *J. Mol. Catal. A*, 2010, **317**, 34; (b) H. W. Huang, J. J. Wang, F. Dong, Y. X. Guo, N. Tian, Y. H. Zhang and T. R. Zhang, *Cryst. Growth Des.*, 2015, **15**, 534; (c) Z. Y. Zhao, Y. Zhou, F. Wang, K. H. Zhang, S. Yu and K. Cao, *ACS Appl Mater Interfaces.*, 2015, **7**, 730; (d) H. W. Huang, X. W. Li, J. J. Wang, F. Dong, P. K. Chu, T. R. Zhang and Y. H. Zhang, *ACS Catal.*, 2015, **5**, 4094; (e) D. D. Hu, K. Y. Zhang, Q. Yang, M. J. Wang, Y. Xi and C. G. Hu, *Appl. Surf. Sci.*, 2014, **316**, 93.
8 C. Greaves and S. K. Blower, *Mater. Res. Bull.*, 1988, **23**, 1001.
9 C. F. Guo, J. M. Zhang, Y. Tian and Q. Liu, *ACS Nano*, 2012, **6**, 8746.
10 Y. Zhou, H. Y. Wang, M. Sheng, Q. Zhang, Z. Y. Zhao, Y. H. Lin, H. F. Liu and G. R. Patzke, *Sens. Actuators B*, 2013, **188**, 1312.
11 G. Q. Zhu, J. Lian, M. Hojamberdiev and W. X. Que, *J. Clust. Sci.*, 2013, **24**, 829.
12 H. Liu, M. Luo. J. C. Hu, T. F. Zhou, R. Chen and J. L. Li, *Appl. Catal. B*, 2013, **140-141**, 141.
13 Y. H. Lei and Z. X. Chen, *J. Chem. Phys.*, 2013, **138**, 054703.
14 L. Chen, R. Huang, S. F. Yin, S. L. Luo and C. T. Au, *Chem. Eng. J.*, 2012, **193-194**, 123-130.
15 H.-Y. Jiang, P. Li, G. G. Liu, J. H. Ye and J. Lin, *J. Mater. Chem. A,* 2015, **3**, 5119.
16 (a) P. Madhusudan, J. R. Ran, J. Zhang, J. G. Yu and G. Liu, *, Appl. Catal. B*, 2011, **110**, 286; (b) X. F. Cao, L. Zhang, X. T. Chen and Z. L. Xue, *CrystEngComm*, 2011, **13**, 1939; (c) Y. Zheng, F. Duan, M. Q. Chen and Y. Xie, *J. Mol. Catal. A*, 2010, **317**, 34; (d) S. Q. Liu, Y. Q. Tu and G. D. Dai, *Ceram. Int.*, 2014, **40**, 2343.
17 M. N. Gómez-Cerezo, M. J. Muñoz-Batista, D. Tudela, M. Fernández-García and A. Kubacka, *Appl. Catal. B*, 2014, **156-157**, 307.
18 S. Shamaila, A. K. L. Sajjad, F. Chen and J. L. Zhang, *Appl. Catal. B*, 2010, **94**, 272.
19 F. Dong, S. C. Lee, Z. B. Wu, Y. Huang, M. Fu, W.-K. Ho, S. C. Zou and B. Wang, *J. Hazard. Mater.*, 2011, **195**, 346.
20 (a) P. Madhusudan, J. Yu, W. Wang, B. Cheng and G. Liu, *Dalton Trans.*, 2012, **41**, 14345; (b) P. Madhusudan, J. Zhang, B. Cheng and G. Liu, *CrystEngComm*, 2013, **15**, 231.
21 S. W. Liu, J. G. Yu and M. Jaroniec, *Chem. Mater.*, 2011, **23**, 4085.
22 (a) H. Kim, P. Borse, W. Choi and J. Lee, *Angew. Chem. Int. Ed.*, 2005, **44**, 4485; (b) Q. Zhang, Y. Zhou, F. Wang, F. Dong, W. Li, H. M. Li and G. R. Patzke, *J. Mater. Chem. A*, 2014, **2**, 11065.
23 A. Cabot, A. Marsal, J. Arbiol and J. R. Morante, *Sens. Actuators B*, 2004, **99**, 74.
24 (a) R. P. Hu, X. Xiao, S. H. Tu, X. X. Zuo and J. M. Nan, *Appl. Catal. B*, 2015, **163**, 510; (b) G. Y. Cai, L. L. Xu, B. Wei, J. X. Che, H. Gao and W. J. Sun, *Mater. Lett.*, 2014, **120**, 1.

Photocatalytically active β-Bi_2O_3 nanosheets exposed with active {001} facets was facilely prepared through annealing $Bi_2O_2CO_3$ with thermal stable {001} facets.